COLD SPRING HARBOR
Molecular Case Studies

RESEARCH REPORT

Whole-genome characterization of myoepithelial carcinomas of the soft tissue

Joanna Cyrta,[1,2,7,9] Joel Rosiene,[2,3,9] Rohan Bareja,[2,4] Sarah Kudman,[1,2] Wael Al Zoughbi,[1,2] Samaneh Motanagh,[1,2] David C. Wilkes,[2] Kenneth Eng,[2,4] Tuo Zhang,[2,4] Evan Sticca,[2,4] Susan Mathew,[1] Mark A. Rubin,[1,2,8] Andrea Sboner,[1,2,4] Olivier Elemento,[1,2,4] Brian P. Rubin,[5] Marcin Imielinski,[1,2,6,10] and Juan Miguel Mosquera[1,2,6,10]

[1]Department of Pathology and Laboratory Medicine, Weill Cornell Medicine, New York, New York 10021, USA; [2]Caryl and Israel Englander Institute for Precision Medicine, Weill Cornell Medicine and New York Presbyterian, New York, New York 10021, USA; [3]SUNY Downstate College of Medicine, Brooklyn, New York 11203, USA; [4]Institute for Computational Biomedicine, Weill Cornell Medicine, New York, New York 10021, USA; [5]Department of Pathology, Cleveland Clinic, Cleveland, Ohio 44195, USA; [6]New York Genome Center, New York, New York 10013, USA

Abstract Myoepithelial carcinomas (MECs) of soft tissue are rare and aggressive tumors affecting young adults and children, but their molecular landscape has not been comprehensively explored through genome sequencing. Here, we present the whole-exome sequencing (WES), whole-genome sequencing (WGS), and RNA sequencing findings of two MECs. Patients 1 and 2 (P1, P2), both male, were diagnosed at 27 and 37 yr of age, respectively, with shoulder (P1) and inguinal (P2) soft tissue tumors. Both patients developed metastatic disease, and P2 died of disease. P1 tumor showed a rhabdoid cytomorphology and a complete loss of INI1 (SMARCB1) expression, associated with a homozygous *SMARCB1* deletion. The tumor from P2 showed a clear cell/small cell morphology, retained INI1 expression and strong S100 positivity. By WES and WGS, tumors from both patients displayed low tumor mutation burdens, and no targetable alterations in cancer genes were detected. P2's tumor harbored an *EWSR1::KLF15* rearrangement, whereas the tumor from P1 showed a novel *ASCC2::GGNBP2* fusion. WGS evidenced a complex genomic event involving mainly Chromosomes 17 and 22 in the tumor from P1, which was consistent with chromoplexy. These findings are consistent with previous reports of *EWSR1* rearrangements (50% of cases) in MECs and provide a genetic basis for the loss of SMARCB1 protein expression observed through immunohistochemistry in 10% of 40% of MEC cases. The lack of additional driver mutations in these tumors supports the hypothesis that these alterations are the key molecular events in MEC evolution. Furthermore, the presence of complex structural variant patterns, invisible to WES, highlights the novel biological insights that can be gained through the application of WGS to rare cancers.

[Supplemental material is available for this article.]

Corresponding author:
jmm9018@med.cornell.edu;
mski@mskilab.org

Ontology term: myoepithelial carcinoma

Published by Cold Spring Harbor Laboratory Press

doi:10.1101/mcs.a006227

[7]Present address: Department of Pathology, Institut Curie, PSL University, 75005 Paris, France
[8]Present address: Department for BioMedical Research, University of Bern, 3008, Bern, Switzerland
[9]These authors contributed equally to this work.
[10]These authors share senior authorship.

INTRODUCTION

A key challenge in the clinical management of very rare cancers (<1 case per 100,000 person-years) is that very little is known about targetable alterations that these tumors may harbor. As a result, patients with very rare cancers do not benefit from therapeutic innovations that have been tailored to the molecular features of more common tumor types. More fundamentally, it is uncertain which of these rare cancers, often defined primarily on the basis of histomorphology, represent molecular cohesive disease entities.

Myoepithelial carcinomas (MECs) of soft tissue and skin are very rare tumors with an incidence rate of 0.0018 (soft tissue) and 0.0007 (skin) per 100,000 person-years (Zhang et al. 2017) that mainly affect young adults, and ~20% of cases occur in children (Gleason and Fletcher 2007; Jo and Fletcher 2015; Jo 2020). They have an aggressive clinical course, with local recurrence or metastases reported in 40%–50% of cases, and the therapeutic approach is not well-codified (Jo and Fletcher 2015). In the World Health Organization (WHO) 2020 classification of Soft Tissue and Bone Tumours, MECs are included in the chapter "tumors of uncertain differentiation," possibly because their cellular counterpart in normal mesenchymal tissue has not been identified (WHO 2020). Because of a wide range of possible cytological, architectural, and immunophenotypic features (Suurmeijer et al. 2020), MECs represent a heterogeneous and still evolving entity and may prove to be under-diagnosed.

Recurrent genomic alterations, which frequently involve the 22q11–12 region, have been identified in MECs by fluorescence in situ hybridization (FISH) and chromosome banding analysis, as well as Sanger sequencing over the *EWSR1* locus. About 50% of cases harbor rearrangements of *EWSR1* (Antonescu et al. 2010; Jo and Fletcher 2015) with various possible 3′ fusion partners (Brandal et al. 2008, 2009; Antonescu et al. 2010; Agaram et al. 2015; Huang et al. 2015; Cajaiba et al. 2016; Stevens et al. 2018) or, alternatively, rearrangements of *FUS* (Huang et al. 2015), a paralog of *EWSR1* located on Chromosome 16. The second recurrent molecular finding demonstrated by immunohistochemistry is the loss of expression of SMARCB1 (also known as INI-1 or BAF47) (Gleason and Fletcher 2007; Hornick et al. 2009; Le Loarer et al. 2014), a core subunit of the SWI/SNF chromatin remodeling complex, observed in up to 40% of MECs and associated with *SMARCB1* deletions in a subset of cases (Le Loarer et al. 2014).

Despite the identification of the above recurrent molecular events, a complete genomic landscape of MEC has not been reported to date. As a result, it is unclear whether additional driver alterations may play a role in MEC evolution. Soft tissue tumors are generally enriched in structural variations (Cortés-Ciriano et al. 2020), much of which are invisible to targeted genomic profiling including panel and whole-exome sequencing (WES). This suggests that more comprehensive sequencing might be helpful in uncovering novel MEC drivers. To address this knowledge gap, we performed WES, whole-genome (WGS), and RNA sequencing (RNA-seq) on two MEC cases from our institution.

RESULTS

Clinicopathological Findings

Patient characteristics and outcomes are summarized in Table 1.

Histopathologic analysis was performed for 12 samples (Table 1), comprising one primary tumor sample for each patient and five samples of metastases or local recurrence for each patient. Morphological and immunohistochemical features of all samples were consistent with MEC. This included trabecular architecture and the presence of myxoid stroma, observed across all tumor samples (Fig. 1). However, morphological and immunohistochemical

Table 1. Clinical characteristics of the two patients with myoepithelial carcinoma and summary of available samples

	Age at diagnosis	Primary tumor	Metastatic and/or recurrent samples	Outcome
Patient 1 (WCM791)	27 yr	Soft tissue, shoulder (MEC1) sample 1	Axillary lymph node (sample 2) Local recurrence (sample 3) Chest wall recurrence 1 (sample 4) Chest wall recurrence 2 (sample 5) Supra-clavicular lymph node (sample 6)	Alive with metastatic disease
Patient 2 (WCM790)	37 yr	Soft tissue, inguinal (MEC2) sample 1	Pleura (sample 2) Liver (sample 3) Adrenal (sample 4) Para-aortic lymph node (sample 5) Brain (sample 6)	Died of disease

differences were also noted between the two patients, in keeping with the heterogeneous nature of MEC (Suurmeijer et al. 2020). Tumor samples from Patient 1 showed a prominent plasmacytoid or rhabdoid cytology and a complete loss of nuclear INI-1 expression. In contrast, tumor samples from Patient 2 showed small round cell and clear cell cytology, a biphasic growth pattern, strong diffuse S100 expression, and retained INI-1 expression. Notably, these distinct histopathologic features were stable from primary tumor to metastasis for each patient. All IHC findings are summarized in Table 2, and were also consistent across samples from each patient.

SMARCB1 deficiency is seen in >95% of malignant rhabdoid tumors (RTs) (Versteege et al. 1998), and up to 70% of RTs show loss of expression of another SWI/SNF subunit, SMARCA2 (BRM) (Kahali et al. 2014). To investigate possible similarities between MECs and RTs, we assessed BRM expression in MEC using immunohistochemistry (IHC). In both cases, BRM showed a heterogeneous staining pattern, with alternating areas positive and negative for nuclear BRM expression (Supplemental Fig. S1). Heterogeneous BRM expression has previously been observed in RTs (Yoshida et al. 2017; Andrianteranagna et al. 2021), which could indicate some similarities between MECs and RTs with respect to SWI/SNF biology.

Comprehensive Genomic Profiling of MECs

To get a preliminary genomic landscape of MEC, we performed WES on 12 MEC samples from the two patients and normal adjacent tissue (mean coverage: 98.5×, range: 83×–119×). Comparison of tumor samples and normal adjacent tissue demonstrated low tumor mutational burden across all MEC samples (mean 1.35 mutations/Mb, range 0.43–2.98), including the metastatic/recurrent samples (Supplemental Fig. S2). Results are summarized in Supplemental Table S1. Only a few variants in Tier 1 or 2 genes (as per COSMIC Cancer Gene Census) were found, including a p.E830G missense *POLE* mutation (predicted as probably damaging by the PolyPhen-2 tool) in three samples from Patient 2; a p.R1239P *NUMA1* mutation (probably damaging) in Patient 2—sample 5; a *LARP4B* p.V449F (probably damaging) in Patient 2—sample 4; and a few other variants all predicted as "benign."

Soft tissue sarcomas, including Ewing sarcoma, have been previously associated with high burdens of complex structural variants (SVs) (Anderson et al. 2018). Because WES is limited in its ability to assess SVs, we used WGS to profile the primary MEC tumors from Patients 1 and 2 (median Patient 1 tumor coverage—29×, Patient 2—22×) and their matched benign tissue (median Patient 1 normal coverage—25×, Patient 2—15×). Analysis of somatic mutations, gene dosage, and gene fusions revealed five alterations in known cancer genes as

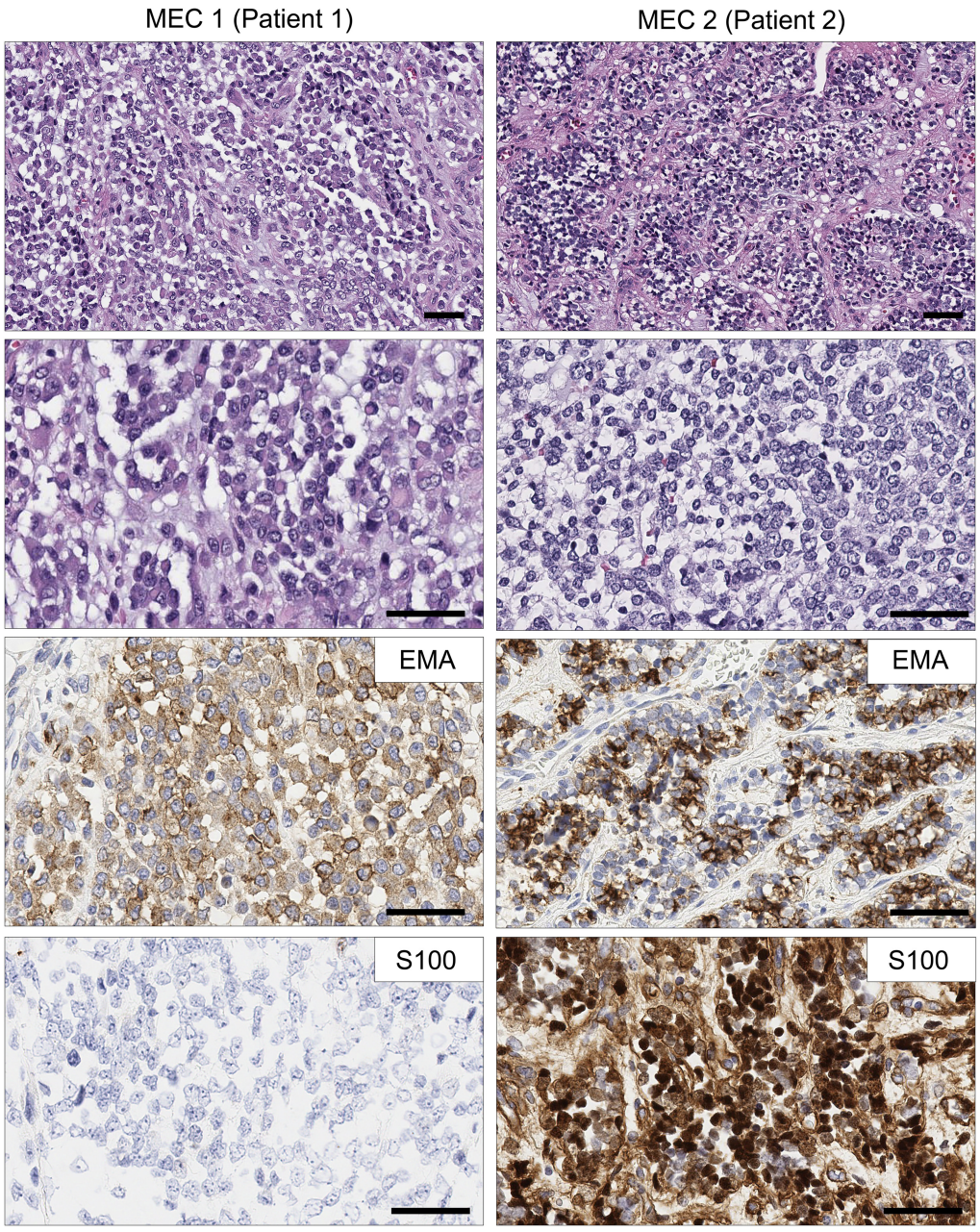

Figure 1. Histomorphology (HE) and representative immunostainings in the two cases: Patient 1, plasmacytoid and rhabdoid cytology, positive epithelial membrane antigen (EMA) staining, and negative S100 staining; Patient 2, small cell and clear cell cytology, positive EMA, and S100 staining. Scale bar, 50 µm.

annotated by the Sanger Cancer Gene Census (Fig. 2A; Table 3). Notably, the MEC from Patient 1 (MEC1) harbored a homozygous loss of *SMARCB1* and *NF1*, whereas the MEC from Patient 2 (MEC2) showed an in-frame *EWSR1* (Chr 22)::*KLF15* (Chr 3) fusion, consistent with previous studies. MEC2 additionally showed a missense mutation of *CREB1*, an *EWSR1* fusion partner in other soft tissue sarcomas. MEC2 harbored a high level (>10 copy) amplification of *ELK4*, an ETS family transcription factor that is a target of oncogenic *cis*-splicing in

Table 2. Summary of immunohistochemical findings and *SMARCB1* FISH results in tumors from the two patients (primary samples) with myoepithelial carcinoma

	EMA	Pan-CK	SMA	S100	GFAP	p63	INI-1 (*SMARCB1*)	BRM (*SMARCA2*)	*SMARCB1* FISH
Patient 1 (WCM791)	+++	+	–	–	+/–	–	Lost	++ (alternating)	Homozygous deletion
Patient 2 (WCM790)	++	+/–	–	+++	–	–	Retained	++ (alternating)	No deletion

(FISH) Fluorescence in situ hybridization, (EMA) epithelial membrane antigen, (Pan-CK) pan cytokeratin, (SMA) smooth muscle actin, (GFAP) glial fibrillary acidic protein, (+++) diffuse positivity, (++) heterogeneous (patchy) positivity, (+) focal positivity (10% of tumor cells), (+/–) positive in isolated cells, (–) negative.

prostate cancer (Zhang et al. 2012); this was also confirmed by WES in all samples from this patient.

Mutational Signatures in MECs

Mutational signature analysis (Fig. 2A) revealed a substantial fraction of single-nucleotide variants (SNVs) in both patients with COSMIC Signature 3, a trinucleotide context SNV pattern that has previously been associated with homologous recombination (HR) deficiency, and a defect in DNA repair (Polak et al. 2017). Some 36.8% and 17.4% of SNVs were attributable to Signature 3 in MEC1 and MEC2, respectively. We examined both MEC genomes for somatic alterations in genes encoding the HR pathway and other genome integrity factors; however, no such alterations were detected with a high level of confidence.

Complex SV Patterns in MECs

Although both genomes were nearly diploid (Fig. 2A), they harbored a large spectrum of structural variants, including simple events (translocations, duplications, deletions, and inversions) and more complex patterns (templated insertion chains, chromoplexy, chromothripsis, and double minutes) (Fig. 2B). Examining the MEC1 genome for additional protein-coding structural variants revealed a fusion of the 5′ portion of *ASCC2*, which encodes Activating Signal Cointegrator 1 Complex Subunit 2 (Chr 22), to the 3′ portion of *GGNBP2*, which encodes a zinc finger DNA binding protein Gametogenetin Binding Protein 2 (Chr 17). Notably, in MEC1, the loss of *SMARCB1* and *NF1* as well as the *ASCC2::GGNBP2* fusion appeared to be part of the same complex SV cluster targeting Chromosomes 17 and 22 and

Table 3. High-impact variants by projected loss of function detected in two myoepithelial carinomas

Patient	Sample	Gene	Chromosome	HGVS DNA Reference
Patient_1	WCM791_sample_1_MEC1	*C11orf57*	11	c.344_345delAG
Patient_1	WCM791_sample_1_MEC1	*ZNF573*	19	c.986delC
Patient_2	WCM790_sample_1_MEC2	*MACF1*	1	c.9012_9015dupAGAC
Patient_2	WCM790_sample_1_MEC2	*OR52I1*	11	c.704dupA
Patient_2	WCM790_sample_1_MEC2	*MRPL48*	11	c.378_382delAATGC
Patient_2	WCM790_sample_1_MEC2	*RNPS1*	16	c.638delC
Patient_2	WCM790_sample_1_MEC2	*MAP2K6*	17	c.420C > A
Patient_2	WCM790_sample_1_MEC2	*PRR12*	19	c.502dupC
Patient_2	WCM790_sample_1_MEC2	*ZNF513*	2	c.799 + 2_799 + 4delTAA
Patient_2	WCM790_sample_1_MEC2	*C22orf29*	22	c.6_13delTCGTGGCC
Patient_2	WCM790_sample_1_MEC2	*NPTX2*	7	c.1006delG
Patient_2	WCM790_sample_1_MEC2	*PLEC*	8	c.1720delG

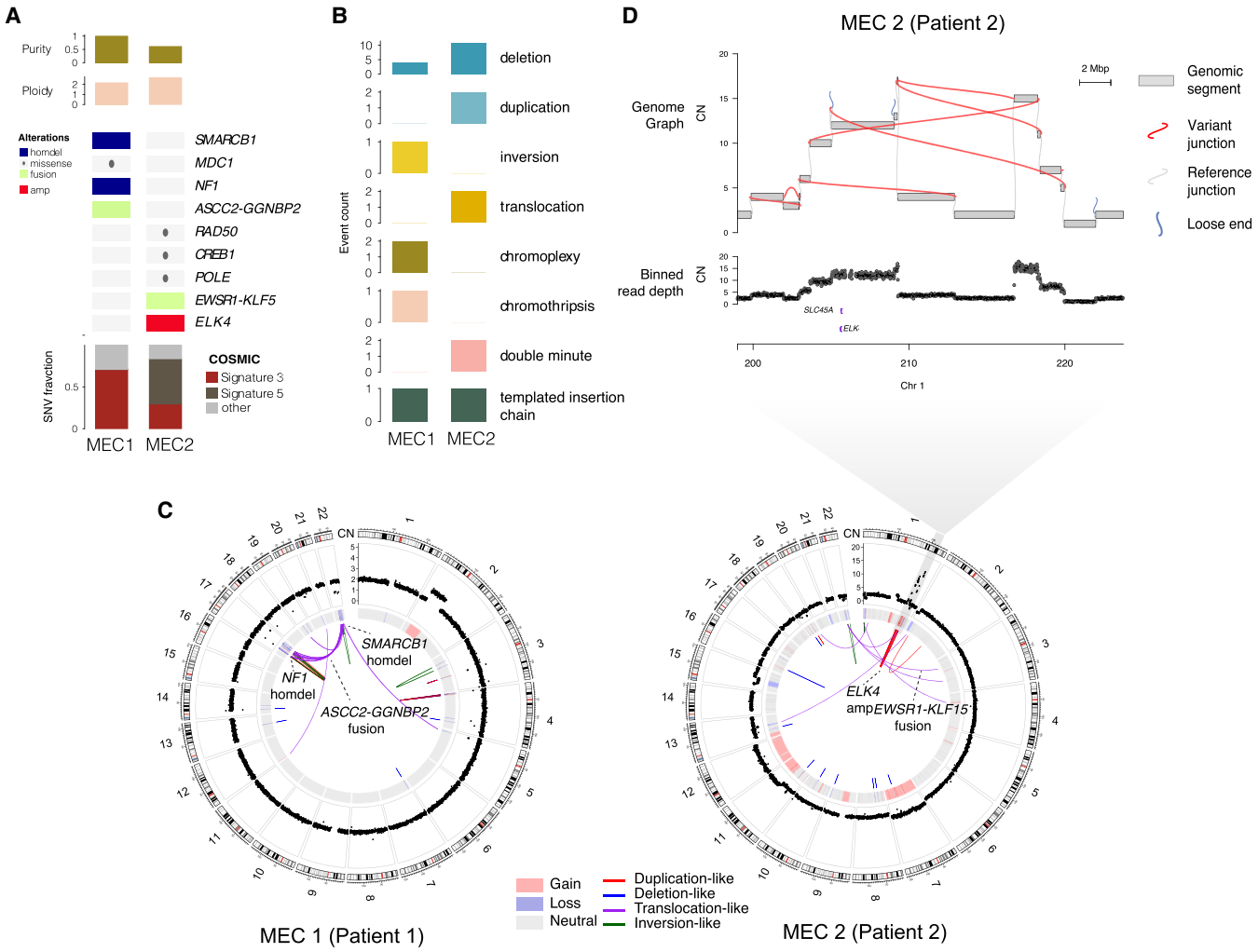

Figure 2. Whole-genome sequencing (WGS) landscape of two myoepithelial carcinoma (MEC) cases. (*A*) Matrix of key genomic alterations, purity, ploidy, tumor mutational burden, and single-nucleotide variant (SNV) signatures in MEC1 and MEC2. Purity/ploidy statistics and gene level alterations resulting from SNV and copy-number alterations. (*B*) Counts of distinct classes of structural variants across the two MEC cases. (*C*) CIRCOS plots for both cases showing (from outer to inner) karyogram, binned read depth, segmented copy-number alterations, and rearrangements junctions in the inner circle. (*D*) Zoomed-in view of a complex amplicon on Chr 1 in MEC2, leading to the copy gain of two Cancer Gene Census genes to more than 10 copies each. This includes *ELK4*, which encodes an ETS transcription factor in the TCF family, not previously associated with soft tissue sarcomas.

others, in an otherwise simple genomic background (Fig. 2C). Similarly, the *ELK4* amplification in MEC2 was the result of a complex, nested, and focal pattern of high-copy duplication junctions on Chromosome 1q, suggestive of a double minute, a type of large extrachromosomal circular DNA (Fig. 2C,D). As with MEC1, the remainder of the MEC2 genome was quiet.

Validation of Gene Fusions Using RNA-seq and FISH

To validate and assess expression of these protein-coding gene fusions, we performed RNA-seq on both MEC1 and MEC2 tumors. Transcriptome analysis (RNA-seq) confirmed

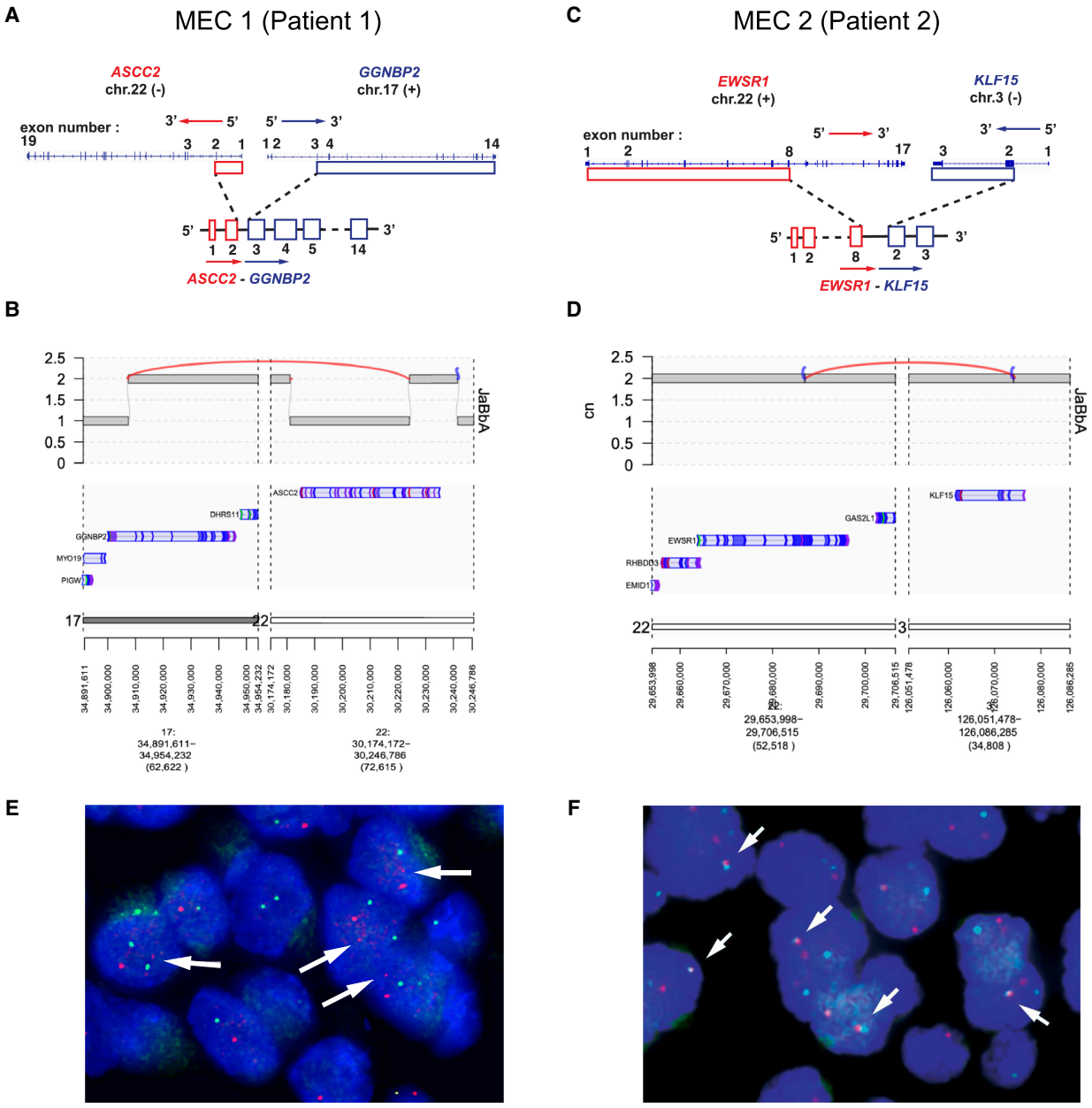

Figure 3. Mapping and validation of protein-coding gene fusions detected in two myoepithelial carcinomas (MECs). Patient 1 (*A*,*B*): A schematic representation of the *ASCC2*::*GGNBP2* gene fusion in MEC1, including exons and introns, but not showing the exact breakpoint (*A*), with corresponding whole-genome sequencing (WGS) representation using JaBbA (*B*). Patient 2 (*C*,*D*): A schematic representation of the *EWSR1*::*KLF15* gene fusion, including exons and introns, but not showing the exact breakpoint (*C*), with corresponding WGS representation using JaBbA (*D*). (*E*) Fluorescence in situ hybridization (FISH) fusion assay for MEC1 (*ASCC2*, red; *GGNBP2*, green), which failed to confirm the fusion, but consistently shows a reduced size of one of the two red signals (arrows). (*F*) FISH fusion assay for MEC2 (*EWSR1*, red; *KLF15*, green), revealing fusion signals (arrows).

expression of the *ASCC2* (exon 2)::*GGNBP2* (exon 3) fusion transcript in MEC1 (Fig. 3A,B), which we additionally validated by reverse transcription-polymerase chain reaction (RT-PCR) followed by Sanger sequencing (Supplemental Fig. S3). Transcriptome analysis also

confirmed the expression of a previously described *EWSR1* (exon 8)::*KLF15* (exon 2) fusion transcript in MEC2 (Fig. 3C,D).

For additional validation of these gene fusions, we performed fusion FISH assays. For the *ASCC2::GGNBP2* fusion in MEC1, combining a telomeric (5′) *ASCC2* probe and a telomeric (3′) *GGNBP2* probe did not reveal a fusion signal; however, it showed that one of the two *ASCC2* signals was smaller in size (Fig. 3E). This was consistent with WGS, which showed a heterozygous deletion at the 5′ end of *ASCC2* (Fig. 3B). A FISH assay combining a centromeric *EWSR1* probe and a centromeric *KLF15* probe confirmed the gene fusion in MEC2 (Fig. 3F).

Comprehensive Analysis of the *SMARCB1* Locus in MEC1

We next sought to investigate in more detail the mechanism of *SMARCB1* and *NF1* locus deletion in MEC1. Visualization of this locus revealed a single large cluster of 32 (primarily) long-range and interchromosomal SV junctions whose break ends were very proximal (within 150 Kbp) to each other (Fig. 4A), causing the loss of both *NF1* and *SMARCB1* (Fig. 4B). FISH confirmed complete absence of the *SMARCB1* gene (Fig. 4C) and IHC showed tumor-specific loss of SMARCB1 protein expression (Fig. 4D). This junction pattern, spanning Chromosomes 17, 19, and 22, was consistent with a large chain of quasi-reciprocal rearrangements called a chromoplexy (Baca et al. 2013), previously observed in Ewing's sarcoma (Anderson et al. 2018). To better understand the evolution of this complex locus, we first analyzed allelic copy number at heterozygous parental single-nucleotide polymorphisms (SNPs). We found only focal loss of heterozygosity across the three affected chromosomes, suggesting that this chromoplexy may have simultaneously rearranged both parental alleles. To address this question more directly, we deconvolved the rearrangement and junction patterns into linear haplotypes using gGnome (Fig. 4A). This analysis revealed six complex derivative chromosomes spanning both parental haplotypes of Chromosomes 17 and 22. We conclude that a single punctuated >30-way rearrangement targeted both parental alleles in MEC1, explaining the biallelic copy loss of *NF1* and *SMARCB1* and the *ASCC2::GGNBP2* fusion.

DISCUSSION

Because of the rarity of soft tissue MECs, diagnostic difficulties related to incomplete characterization of MECs as a group, and a wide range of possible pathologic features, the molecular underpinnings of this entity are challenging to study. Here, we show that MECs display a strikingly low point mutation rate compared to other cancers (Lawrence et al. 2013), consistent with what is often seen in gene fusion–associated malignancies (Yoshihara et al. 2015). Our findings are in keeping with a previous case report of a soft tissue MEC interrogated via targeted sequencing, which found a low mutation burden (1 mutation/Mb) and no alterations in known cancer genes, except for a frameshift in *MAP3K6* (Stevens et al. 2018). Conversely, in the only published case of a soft tissue MEC interrogated through WES, albeit without a germline control, truncating mutations in tumor suppressor genes *RB1* and *MED12* were identified (Hoggard et al. 2017). Our WGS analysis here additionally demonstrates that loss of tumor suppressors in MECs may result from complex structural events, the spectra of which are as yet uncharacterized in MECs.

Complete loss of SMARCB1 (INI-1) expression by IHC is seen in 10%–40% of MECs (Gleason and Fletcher 2007; Hornick et al. 2009; Le Loarer et al. 2014) and can be associated with homozygous *SMARCB1* deletion on FISH (Le Loarer et al. 2014). Consistently, we observed homozygous *SMARCB1* deletion and loss of expression by immunohistochemistry (IHC) in Patient 1. Biallelic inactivation of *SMARCB1*, which encodes a core member of the chromatin remodeling complex SWI/SNF, can be seen in various tumor types, but is

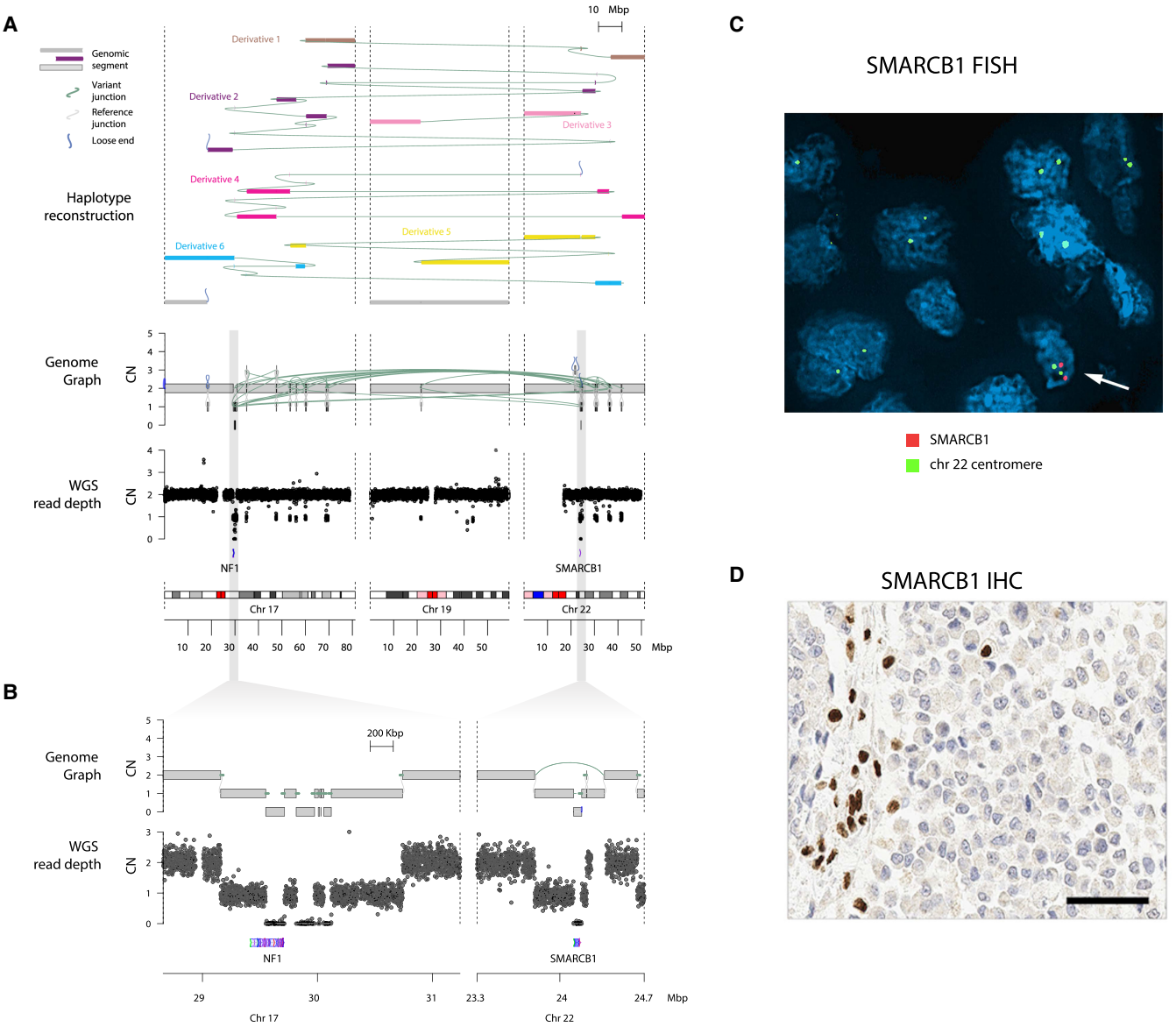

Figure 4. Complex structural variants in MEC1 (Patient 1). (*A*) Genome graph of a biallelic chromoplexy involving Chrs 17, 19, and 22 in MEC1. From bottom, karyogram and normalized binned read depth are plotted across the three chromosomes. The genome graph shows the copy number at genomic regions linked by reference (gray) and variant (green) junctions. Loose ends (blue) represent copy changes that cannot be mapped to a rearrangement. The *top* tracks represent derivative chromosomes, each plotted as a distinctly colored path of genomic segments along the genome, which when summed explain the copy profile. The variant junctions form a reciprocal cluster, all harboring break ends within 150 Kbp of each other, indicating that they likely occurred simultaneously in tumor evolution as a chromoplexy event. These junctions are distributed across six derivative alleles of the three chromosomes, resulting in biallelic deletion *NF1*. SMARCB1 is targeted by an additional deletion junction that may have occurred before or after this complex punctuated event. (*B*) Zoom-in on genome graph (*top*) and read depth (*bottom*) from graph in *A*, showing biallelic inactivation of *NF1* and *SMARCB1*. (*C*) Fluorescence in situ hybridization (FISH) for *SMARCB1* in Patient 1 showing complete absence of the *SMARCB1* locus (red probe) and persistence of the Chr 22 centromere (green); admixed benign cells (arrow) represent positive internal controls. (*D*) Immunohistochemistry (IHC) demonstrates complete loss of nuclear INI-1 (SMARCB1) expression in the tumor cells. Scale bar, 50 µm.

particularly recurrent in malignant rhabdoid tumors, epithelioid sarcomas, and medullary carcinomas of the kidney (Versteege et al. 1998; Le Loarer et al. 2014; Calderaro et al. 2016). In MECs, it remains unclear whether *SMARCB1* inactivation contributes to oncogenesis or whether it is a bystander event due to recurrent alterations of the 22q11–12 region. To our knowledge, we also show for the first time that BRM (SMARCA2) expression follows an "alternating" pattern in MECs, with the existence of a BRM-negative tumor cell population; however, this remains to be confirmed in a larger cohort.

Our WGS results reveal that a >30-way biallelic chromoplexy event may have simultaneously caused biallelic *NF1* loss as well as the loss of *SMARCB1* and a novel *ASCC2*::*GGNBP2* fusion in MEC1. The latter was not supported by FISH, most likely due the resolution of the assay—the region of *ASCC2* involved in the fusion (the first two exons only) is too small to be detected by the FISH probe. Interestingly, the deletion of the second copy of *SMARCB1* involves a simple deletion junction that may have occurred independent of this event. Although chromoplexy is frequent in Ewing sarcoma and prostate cancer (Baca et al. 2013; Anderson et al. 2018), the finding of a punctuated SV that targets both parental homologs is unprecedented, to our knowledge. This finding raises the question of how both parental alleles might get entangled in such a rearrangement, as well as the degree of selective pressures (i.e., for *NF1* and *SMARCB1*) that might raise the probability of such an unlikely event.

Notably, this chromoplexy pattern was also annotated as a chromothripsis. Chromothripsis is the product of chromosome shattering and random loss and religation of DNA segments within micronuclei or in anaphase bridges (Maciejowski et al. 2015; Papathanasiou et al. 2022) and is sometimes difficult to distinguish from chromoplexy. Although the clustered SV patterns and oscillating copy number may qualify this locus as a chromothripsis, the minimal amount of copy-number loss (3.74 Mbp of the 109.8 Mbp of Chromosomes 17 and 22) is less typical for chromothripsis. These observations make chromoplexy a more likely explanation for this pattern. Although the mechanistic basis of chromoplexy is unclear, one candidate is a chain reaction of "half crossovers" mediated by break-induced replication as a consequence of replication fork collapse (Wu and Malkova 2021). The role of chromoplexy and these mutational processes in the evolution of MECs and other soft tissue sarcomas (including Ewing sarcoma) is an exciting area for future investigation.

About 50% of MECs harbor rearrangements of *EWSR1* (Antonescu et al. 2010; Jo and Fletcher 2015), for which the 3′ fusion partners may include *POU5F1*, *PBX1*, *PBX3*, *ZNF444*, *KLF17*, *KLF15*, or *ATF1* (Brandal et al. 2008, 2009; Antonescu et al. 2010; Agaram et al. 2015; Huang et al. 2015; Cajaiba et al. 2016; Stevens et al. 2018). Alternatively, fusions involving *FUS*, a paralog of *EWSR1*, as the 5′ partner and *KLF17* as the 3′ partner, have been described (Huang et al. 2015). The *EWSR1*::*KLF15* rearrangement identified in Patient 2 has previously been reported in six MECs and in one benign myoepithelial tumor, in various anatomic sites (Cajaiba et al. 2016; Stevens et al. 2018; Patel et al. 2019; Suurmeijer et al. 2020; Bodis et al. 2021). In contrast to Patient 2 (age at diagnosis: 37 yr), all previously reported cases occurred in children and adolescents, except for one parotid gland tumor diagnosed at 20 yr (Stevens et al. 2018). Interestingly, previously described tumors and the disease of Patient 2 show microscopic similarities, including a biphasic morphology, a "small round cell" appearance (which may erroneously lead to the diagnosis of Ewing sarcoma), focal clear cell features, diffuse S100 expression, and retained INI-1 expression. Taken together, this case further supports the recently proposed hypothesis that MECs with an *EWSR1*::*KLF15* rearrangement may represent a distinct subgroup of tumors with characteristic pathologic features (Suurmeijer et al. 2020).

The *ASCC2*::*GGNBP2* in-frame fusion transcript identified in Patient 1 (by WGS and RNA-seq) has not been reported to date. *GGNBP2* encodes Gametogenetin Binding Protein 2, a zinc-finger DNA-binding protein also known as ZNF403. Although little is known

about GGNBP2 function, *GGNBP2* knockdown in human cell lines has been shown to result in cell cycle arrest, impair anchorage-independent growth, and decrease cell migration (Guan et al. 2012). Of note, in some recurrent rearrangements previously identified in MECs, the 3′ fusion partner also encodes a zinc finger protein (*KLF17*, *KLF15*, or *ZNF444*) (Brandal et al. 2009; Antonescu et al. 2010; Huang et al. 2015; Cajaiba et al. 2016; Stevens et al. 2018). This raises the possibility that *GGNBP2* fusion may be a proliferative driver in MECs. *ASCC2* (Activating Signal Cointegrator 1 Complex Subunit 2) is part of the ASC-2 transcriptional coactivator complex (Goo et al. 2003; Kong et al. 2003) and may bear functional similarities to *EWSR1* and *FUS* in their roles as regulators of transcription and RNA splicing, although functional studies are needed to assess for this possibility. Intriguingly, Thway et al. (2015) reported a case of soft tissue MEC with a prominent rhabdoid morphology, loss of INI-1 expression and an atypical *EWSR1* break-apart FISH pattern, whereas Le Loarer et al. (2014) reported three MEC cases with rhabdoid features, loss of INI-1 expression, and no *EWSR1* rearrangement. Thus, it could be interesting to investigate the presence of *GGNBP2::ASCC2* fusions in MECs without *EWSR1* rearrangement, in particular those with rhabdoid features. The *ASCC2::GGNBP2* fusion junction in this case exists amongst set of 17–19–22 translocations, which collectively comprise a complex event consistent with chromoplexy.

Although recurrent rearrangements involving the 22q region are a known finding in MEC, we report for the first time WGS results in two MECs, allowing us to better understand the nature of these events. In a recent WGS analysis of 124 cases of Ewing sarcomas, Anderson et al. (2018) provided evidence that all *EWSR1::ERG* fusions and ∼40% of *EWSR1::FLI1* fusions in these tumors arise through complex, loop-like rearrangements involving chromoplexy or chromothripsis (mechanisms of chromosome shattering involving one or multiple chromosomes). The authors extended their analysis to other tumor types and identified similar chromoplectic events in cases of chondromyxoid fibroma, synovial sarcoma, and phosphaturic mesenchymal tumors (Anderson et al. 2018). Based on our WGS findings, MECs may expand the spectrum of tumor types in which gene fusions arise through chromoplectic loop-like rearrangements, rather than via a simple reciprocal fusion. This is consistent with a previous case report of an MEC in which CGH array, which suggested the presence of a complex rearrangement between Chromosomes 3, 22, and possibly some other genomic regions (Stevens et al. 2018). Of note, similar to *EWSR1* and ETS-family genes brought together in Ewing sarcoma, nearly all gene rearrangements reported to date in MEC, including the two described herein, involve two genes with opposing genomic orientations.

Our whole-genome analysis suggests that the molecular landscapes of MECs is not homogenous, which raises fundamental challenges for a tumor that is very rare. A key remaining question is distinction between MECs and Ewing sarcoma, given that both have small round cell morphology and harbor *EWSR1* rearrangements. However, unlike Ewing sarcoma, MECs typically lack CD99 expression and do not show rearrangements of *ERG* or *FLI1*. A second important differential diagnosis is extrarenal malignant rhabdoid tumor (MRT) for MECs that display INI-1 loss and a rhabdoid morphology. Similar to MECs, MRTs also show a low mutation burden (Lawrence et al. 2013) and may harbor alterations at the 22q locus beyond the *SMARCB1* gene (Chun et al. 2016). Further studies are needed to determine biological differences and similarities between MEC and MRT, and the possibility of some degree of molecular overlap between these entities should be considered.

CONCLUSION

We report the molecular characterization of two cases of soft tissue MEC, which revealed low tumor mutation burden and no actionable alterations in known cancer genes, including in

the metastatic and recurrent samples. Instead, we observed genomic rearrangements consistently involving the 22q11–12 region, associated with focal copy-number alterations and gene fusions. Further studies are needed to assess the incidence and significance of *EWSR1::KLF15* fusion and the newly identified *ASCC2::GGNBP2* rearrangement in MEC. The chromoplexy described in the case of Patient 1 is demonstrative that tumorigenesis may arise subsequent to large scale genomic rearrangement, which raises the prospect of inquiry into the mechanisms of instability or preconditions necessary for large-scale events such as these to occur. Analysis of structural genomic variants in other MEC cases may yet uncover patterns of complex variants, which will help to clarify the degree to which large-scale and complex structural events play in the tumorigenesis of this rare tumor type. Additionally, soft tissue MEC likely expands the spectrum of tumors in which gene fusions may arise through complex rearrangements, rather than by simple translocations.

METHODS

Case Selection and Pathologic Examination

The study was performed under institutional review board-approved protocols that include WCM IRB # 1007011157. Two cases of MEC were identified in our surgical pathology archives. Tumor morphology was reviewed by pathologists with expertise in soft tissue pathology (B.P.R., J.M.M.).

WES

WES was performed on one fresh-frozen and five formalin-fixed paraffin-embedded (FFPE) samples from Patient 1 (P1), on six FFPE samples from Patient 2 (P2), and on benign FFPE tissue for both patients (germline control). We used a previously described (Rennert et al. 2016; Beltran et al. 2015) clinical-grade WES test (EXaCT-1). Briefly, DNA was extracted using Promega Maxwell 16 MDX. Libraries were constructed using targeted capture of 21,522 genes with the HaloPlex System (Agilent), followed by paired-end 2 × 100 bp sequencing with Illumina HiSeq2500, for an intended mean target exome coverage of 80× for both the tumor and the germline samples. Reads were aligned to the human genome (reference GRC37/hg19) and data were analyzed using an internally developed pipeline (Rennert et al. 2016).

RNA-seq

RNA-seq was performed on one fresh-frozen sample from P1 and one FFPE sample from P2. RNA was extracted using Promega Maxwell 16 MDX and RNA integrity was verified using the Agilent Bioanalyzer 2100 (Agilent Technologies). cDNA was synthesized from total RNA using Superscript III (Invitrogen). Sequencing was performed using Illumina HiSeq2500 in 2 × 75 bp paired-end mode, and generated an average of 45 million reads per sample. All reads were independently aligned with STAR_2.4.0f for sequence alignment against the human genome build hg19, downloaded via the UCSC genome browser (http://hgdownload.soe.ucsc.edu/goldenPath/hg19/bigZips/), and SAMTOOLS v0.1.19 for sorting and indexing reads (Li et al. 2009). For fusion analysis, we used STAR-fusion (STAR-Fusion_v0.5.1) and FusionCatcher (v0.99.3e). Fusions with significant support of junction reads and spanning pairs were selected and manually reviewed.

IHC

IHC was performed on sections of FFPE tumor tissue using a Bond III automated immunostainer and the Bond Polymer Refine detection system (Leica Microsystems). Slides were

deparaffinized, and heat-mediated antigen retrieval using the Bond Epitope Retrieval 1 solution at pH6 (H1) or Bond Epitope Retrieval 2 solution at pH9 (H2) or enzyme-mediated antigen retrieval (E1) was performed. The following antibodies and conditions (dilution, antigen retrieval solution, antigen retrieval time) were used: anti-INI-1 (BD Bioscience bd612110, 1/100 H2, 30 min), anti-EMA (Leica PA0035, H1, 20 min), anti-pancytokeratin (Leica PA0909. RTU, Enzyme Treatment, 10 min), anti-SMA (Leica PA0943, RTU, no pretreatment), anti-S100 (Leica PA0900, RTU, Enzyme Treatment, 10 min), anti-GFAP (Leica PA0026, RTU, H2, 20 min), anti-p63 (Biogenex, clone 4A4, 1/50, H2, 30 min), and anti-Brm (Cell Signaling Technology, clone D9E8B, 1/200, ER1, 30 min). Immunostains were evaluated by two study pathologists (J.M.M. and J.C.).

WGS

WGS was performed on one fresh-frozen sample from Patient 1 and one FFPE sample from Patient 2. Library preparation and WGS was performed at the New York Genome Center (NYGC) to a target 80× tumor and 40× normal coverage. Short-read genomic DNA library preparation was performed with the TruSeq DNA PCR-free Library Prep Kit (Illumina). Quality control was assayed for the final libraries with the Agilent 2100 Bioanalyzer by using the DNA 1000 chip (Agilent Technologies). Quality control determined that libraries contained an average peak height (fragment size) of 400 bp. Libraries were sequenced on HiSeq X machines (Illumina) to generate paired-end 2 × 150 bp reads. Reads were aligned to the GRCh37/hg19 reference using Burrows–Wheeler aligner software (Li and Durbin 2009) (bwa aln, v.0.7.8). Best practices for postalignment data processing were followed through use of Picard (https://broadinstitute.github.io/picard/) tools to mark duplicates, the GATK (v.2.7.4) (https://software.broadinstitute.org/gatk/) IndelRealigner module, and GATK base quality recalibration. Junction balanced allelic genome graphs were constructed from junctions and coverage data using the JaBbA (Hadi et al. 2020) tool. Subsequent calling of complex structural events was performed based on characteristics of identified junction clusters. To identify rearranged derivative alleles, walk reconstruction was performed across clusters of junctions with break ends within 150 kb on the genome graph using the gGnome peel function as previously described (Hadi et al. 2020).

FISH

FISH was performed on 4 µm FFPE tissue sections; the complete protocol is described in Supplemental Methods. Dual FISH probes for the *SMARCB1* deletion assay were prepared using BAC clones RP11-71G19 (*SMARCB1*) labeled red and RP11-551L12 (control probe, i.e., telomeric *EWSR1* or 22q12.2) labeled green (BACPAC Resources). For *ASCC2::GGNBP2* and *EWSR1::KLF15* fusion assays, probes labeled with fluorophores were provided by Empire Genomics (Williamsville), and the following BACs were used: RP11-794O14 (*ASCC2*, orange), RP11-141B22 (*GGNBP2*, green), RP11-367E7 (*EWSR1*, orange) and RP11-319C18 (*KLF15*, green).

RT-PCR and Sanger Sequencing

RNA was isolated from tumor tissue and cDNA generated using qScript cDNA SuperMix (QuantaBio). For the *ASCC2::GGNBP2* fusion transcript, PCR amplification was performed using a fusion-specific primer pair (forward: 5′-ACTCCAGATCACCCACAAGG-3′; reverse: 5′-GGGACAAGCTGAGAAAGTGC-3′). Sanger sequencing was performed using the same primers for forward and reverse sequencing, respectively.

ADDITIONAL INFORMATION

Data Deposition and Access

WES data can be found at the publicly accessible repository cbioportal.org. Interpreted WGS variants were submitted to ClinVar (https://www.ncbi.nlm.nih.gov/clinvar/) and can be found under accession numbers SCV002758653–SCV002758746. WES data were deposited to cBioPortal (study reference: stmyec_wcm_2022).

Ethics Statement

Research was conducted under WCM IRB protocol #1007011157 (Comprehensive Cancer Characterization by Genomic and Transcriptomic Profiling), which allows for utilization of next-generation sequencing of de-identified biospecimens. Following the NIH Genomic Data Sharing (GDS) policy, informed consent is not required to generate genomic data from research or clinical specimens collected before January 25, 2015). Further, one of the two patients is now deceased.

Competing Interest Statement

The authors have declared no competing interest.

Referees

Patience Odeniyide
Anonymous

Received June 18, 2022;
accepted in revised form
October 28, 2022.

Acknowledgments

The authors are thankful to the Center for Translational Pathology at the WCM Department of Pathology and Laboratory Medicine (Mai Ho, Leticia Dizon, Bing He) for technical assistance and support and to colleagues of the Computational Biology team (Alexandros Sigaras, Pooja Chandra, Jeffrey M. Tang, and Noah Greco) for their assistance to create the cBioPortal cohort.

Funding

This project was supported by the Caryl and Israel Englander Institute for Precision Medicine at Weill Cornell Medicine.

REFERENCES

Agaram NP, Chen HW, Zhang L, Sung YS, Panicek D, Healey JH, Nielsen GP, Fletcher CD, Antonescu CR. 2015. *EWSR1-PBX3*: a novel gene fusion in myoepithelial tumors. *Genes Chromosomes Cancer* **54:** 63–71. doi:10.1002/gcc.22216

Anderson ND, de Borja R, Young MD, Fuligni F, Rosic A, Roberts ND, Hajjar S, Layeghifard M, Novokmet A, Kowalski PE, et al. 2018. Rearrangement bursts generate canonical gene fusions in bone and soft tissue tumors. *Science* **361:** eaam8419. doi:10.1126/science.aam8419

Andrianteranagna M, Cyrta J, Masliah-Planchon J, Nemes K, Corsia A, Leruste A, Holdhof D, Kordes U, Orbach D, Corradini N, et al. 2021. SMARCA4-deficient rhabdoid tumours show intermediate molecular features between SMARCB1-deficient rhabdoid tumours and small cell carcinomas of the ovary, hypercalcaemic type. *J Pathol* **255:** 1–15. doi:10.1002/path.5705

Antonescu CR, Zhang L, Chang NE, Pawel BR, Travis W, Katabi N, Edelman M, Rosenberg AE, Nielsen GP, Dal Cin P, et al. 2010. *EWSR1-POU5F1* fusion in soft tissue myoepithelial tumors. A molecular analysis of sixty-six cases, including soft tissue, bone, and visceral lesions, showing common involvement of the *EWSR1* gene. *Genes Chromosomes Cancer* **49:** 1114–1124. doi:10.1002/gcc.20819

Baca SC, Prandi D, Lawrence MS, Mosquera JM, Romanel A, Drier Y, Park K, Kitabayashi N, MacDonald TY, Ghandi M, et al. 2013. Punctuated evolution of prostate cancer genomes. *Cell* **153:** 666–677. doi:10.1016/j.cell.2013.03.021

Beltran H, Eng K, Mosquera JM, Sigaras A, Romanel A, Rennert H, Kossai M, Pauli C, Faltas B, Fontugne J, et al. 2015. Whole-exome sequencing of metastatic cancer and biomarkers of treatment response. *JAMA Oncol* **1:** 466–474. doi:10.1001/jamaoncol.2015.1313

Bodis S, Kroiss S, Tchinda J, Fritz C, Wagner U, Bode PK. 2021. Myoepithelial carcinoma of soft tissue with an *EWSR1-KLF15* gene fusion in an infant. *Pediatr Dev Pathol* **24:** 371–377. doi:10.1177/1093526621999020

Brandal P, Panagopoulos I, Bjerkehagen B, Gorunova L, Skjeldal S, Micci F, Heim S. 2008. Detection of a t(1;22)(q23;q12) translocation leading to an *EWSR1-PBX1* fusion gene in a myoepithelioma. *Genes Chromosomes Cancer* **47:** 558–564. doi:10.1002/gcc.20559

Brandal P, Panagopoulos I, Bjerkehagen B, Heim S. 2009. t(19;22)(q13;q12) Translocation leading to the novel fusion gene *EWSR1-ZNF444* in soft tissue myoepithelial carcinoma. *Genes Chromosomes Cancer* **48:** 1051–1056. doi:10.1002/gcc.20706

Cajaiba MM, Jennings LJ, Rohan SM, Leuer KM, Anagnost MR, Fahner JB, Fulton BK, Geller JI, Perlman EJ. 2016. Expanding the spectrum of renal tumors in children: primary renal myoepithelial carcinomas with a novel *EWSR1-KLF15* fusion. *Am J Surg Pathol* **40:** 386–394. doi:10.1097/PAS.0000000000000545

Calderaro J, Masliah-Planchon J, Richer W, Maillot L, Maille P, Mansuy L, Bastien C, de la Taille A, Boussion H, Charpy C, et al. 2016. Balanced translocations disrupting *SMARCB1* are hallmark recurrent genetic alterations in renal medullary carcinomas. *Eur Urol* **69:** 1055–1061. doi:10.1016/j.eururo.2015.09.027

Chun HE, Lim EL, Heravi-Moussavi A, Saberi S, Mungall KL, Bilenky M, Carles A, Tse K, Shlafman I, Zhu K, et al. 2016. Genome-wide profiles of extra-cranial malignant rhabdoid tumors reveal heterogeneity and dysregulated developmental pathways. *Cancer Cell* **29:** 394–406. doi:10.1016/j.ccell.2016.02.009

Cortés-Ciriano I, Lee JJ, Xi R, Jain D, Jung YL, Yang L, Gordenin D, Klimczak LJ, Zhang CZ, Pellman DS, et al. 2020. Comprehensive analysis of chromothripsis in 2,658 human cancers using whole-genome sequencing. *Nat Genet* **52:** 331–341. doi:10.1038/s41588-019-0576-7

Gleason BC, Fletcher CD. 2007. Myoepithelial carcinoma of soft tissue in children: an aggressive neoplasm analyzed in a series of 29 cases. *Am J Surg Pathol* **31:** 1813–1824. doi:10.1097/PAS.0b013e31805f6775

Goo YH, Sohn YC, Kim DH, Kim SW, Kang MJ, Jung DJ, Kwak E, Barlev NA, Berger SL, Chow VT, et al. 2003. Activating signal cointegrator 2 belongs to a novel steady-state complex that contains a subset of trithorax group proteins. *Mol Cell Biol* **23:** 140–149. doi:10.1128/MCB.23.1.140-149.2003

Guan R, Wen XY, Wu J, Duan R, Cao H, Lam S, Hou D, Wang Y, Hu J, Chen Z. 2012. Knockdown of ZNF403 inhibits cell proliferation and induces G2/M arrest by modulating cell-cycle mediators. *Mol Cell Biochem* **365:** 211–222. doi:10.1007/s11010-012-1262-6

Hadi K, Yao X, Behr JM, Deshpande A, Xanthopoulakis C, Tian H, Kudman S, Rosiene J, Darmofal M, DeRose J, et al. 2020. Distinct classes of complex structural variation uncovered across thousands of cancer genome graphs. *Cell* **183:** 197–210.e32. doi:10.1016/j.cell.2020.08.006

Hoggard TM, Henderson-Jackson E, Bui MM, Caracciolo J, Teer JK, Yoder S, Binitie O, Gonzalez RJ, Brohl AS, Reed DR. 2017. Myoepithelial carcinoma with *RB1* mutation: remarkable chemosensitivity to carcinoma of unknown origin therapy. *BMC Cancer* **17:** 250. doi:10.1186/s12885-017-3249-x

Hornick JL, Dal Cin P, Fletcher CD. 2009. Loss of INI1 expression is characteristic of both conventional and proximal-type epithelioid sarcoma. *Am J Surg Pathol* **33:** 542–550. doi:10.1097/PAS.0b013e3181882c54

Huang SC, Chen HW, Zhang L, Sung YS, Agaram NP, Davis M, Edelman M, Fletcher CD, Antonescu CR. 2015. Novel *FUS-KLF17* and *EWSR1-KLF17* fusions in myoepithelial tumors. *Genes Chromosomes Cancer* **54:** 267–275. doi:10.1002/gcc.22240

Jo VY. 2020. Soft tissue special issue: myoepithelial neoplasms of soft tissue: an updated review with emphasis on diagnostic considerations in the head and neck. *Head Neck Pathol* **14:** 121–131. doi:10.1007/s12105-019-01109-y

Jo VY, Fletcher CD. 2015. Myoepithelial neoplasms of soft tissue: an updated review of the clinicopathologic, immunophenotypic, and genetic features. *Head Neck Pathol* **9:** 32–38. doi:10.1007/s12105-015-0618-0

Kahali B, Yu J, Marquez SB, Thompson KW, Liang SY, Lu L, Reisman D. 2014. The silencing of the SWI/SNF subunit and anticancer gene BRM in Rhabdoid tumors. *Oncotarget* **5:** 3316–3332. doi:10.18632/oncotarget.1945

Kong HJ, Yu HJ, Hong S, Park MJ, Choi YH, An WG, Lee JW, Cheong J. 2003. Interaction and functional cooperation of the cancer-amplified transcriptional coactivator activating signal cointegrator-2 and E2F-1 in cell proliferation. *Mol Cancer Res* **1:** 948–958.

Lawrence MS, Stojanov P, Polak P, Kryukov GV, Cibulskis K, Sivachenko A, Carter SL, Stewart C, Mermel CH, Roberts SA, et al. 2013. Mutational heterogeneity in cancer and the search for new cancer-associated genes. *Nature* **499:** 214–218. doi:10.1038/nature12213

Le Loarer F, Zhang L, Fletcher CD, Ribeiro A, Singer S, Italiano A, Neuville A, Houlier A, Chibon F, Coindre JM, et al. 2014. Consistent *SMARCB1* homozygous deletions in epithelioid sarcoma and in a subset of myoepithelial carcinomas can be reliably detected by FISH in archival material. *Genes Chromosomes Cancer* **53:** 475–486. doi:10.1002/gcc.22159

Li H, Durbin R. 2009. Fast and accurate short read alignment with Burrows–Wheeler transform. *Bioinformatics* **25:** 1754–1760. doi:10.1093/bioinformatics/btp324

Li H, Handsaker B, Wysoker A, Fennell T, Ruan J, Homer N, Marth G, Abecasis G, Durbin R, Subgroup Genome Project Data Processing. 2009. The Sequence Alignment/Map format and SAMtools. *Bioinformatics* **25:** 2078–2079. doi:10.1093/bioinformatics/btp352

Maciejowski J, Li Y, Bosco N, Campbell PJ, de Lange T. 2015. Chromothripsis and kataegis induced by telomere crisis. *Cell* **163:** 1641–1654. doi:10.1016/j.cell.2015.11.054

Papathanasiou S, Mynhier NA, Liu S, Jacob E, Stokasimov E, van Steensel B, Zhang C-Z, Pellman D. 2022. Transgenerational transcriptional heterogeneity from cytoplasmic chromatin. bioRxiv doi:10.1101/2022.01.12.475869

Patel P, Roberts R, Cole J, Stalling M, Nicol K, Hor K, Bowman J, Setty B. 2019. A rare case of an intracardiac myoepithelial carcinoma in an infant. *J Pediatr Hematol Oncol* **41:** e206–e209. doi:10.1097/MPH.0000000000001343

Polak P, Kim J, Braunstein LZ, Karlic R, Haradhavala NJ, Tiao G, Rosebrock D, Livitz D, Kubler K, Mouw KW, et al. 2017. A mutational signature reveals alterations underlying deficient homologous recombination repair in breast cancer. *Nat Genet* **49:** 1476–1486. doi:10.1038/ng.3934

Rennert H, Eng K, Zhang T, Tan A, Xiang J, Romanel A, Kim R, Tam W, Liu YC, Bhinder B, et al. 2016. Development and validation of a whole-exome sequencing test for simultaneous detection of point mutations, indels and copy-number alterations for precision cancer care. *NPJ Genom Med* **1:** 16019. doi:10.1038/npjgenmed.2016.19

Stevens TM, Qarmali M, Morlote D, Mikhail FM, Swensen J, Gatalica Z, Siegal GP, Conry RM. 2018. Malignant Ewing-like neoplasm with an *EWSR1-KLF15* fusion: at the crossroads of a myoepithelial carcinoma and a Ewing-like sarcoma. a case report with treatment options. *Int J Surg Pathol* **26:** 440–447. doi:10.1177/1066896918755009

Suurmeijer AJH, Dickson BC, Swanson D, Zhang L, Sung YS, Fletcher CD, Antonescu CR. 2020. A morphologic and molecular reappraisal of myoepithelial tumors of soft tissue, bone, and viscera with *EWSR1* and *FUS* gene rearrangements. *Genes Chromosomes Cancer* **59:** 348–356. doi:10.1002/gcc.22835

Thway K, Bown N, Miah A, Turner R, Fisher C. 2015. Rhabdoid variant of myoepithelial carcinoma, with *EWSR1* rearrangement: expanding the spectrum of *EWSR1*-rearranged myoepithelial tumors. *Head Neck Pathol* **9:** 273–279. doi:10.1007/s12105-014-0556-2

Versteege I, Sevenet N, Lange J, Rousseau-Merck MF, Ambros P, Handgretinger R, Aurias A, Delattre O. 1998. Truncating mutations of hSNF5/INI1 in aggressive paediatric cancer. *Nature* **394:** 203–206. doi:10.1038/28212

WHO. 2020. *WHO Classification of Tumours: Soft Tissue and Bone Tumours*, 5th edn.

Wu X, Malkova A. 2021. Break-induced replication mechanisms in yeast and mammals. *Curr Opin Genet Dev* **71:** 163–170. doi:10.1016/j.gde.2021.08.002

Yoshida A, Kobayashi E, Kubo T, Kodaira M, Motoi T, Motoi N, Yonemori K, Ohe Y, Watanabe SI, Kawai A, et al. 2017. Clinicopathological and molecular characterization of SMARCA4-deficient thoracic sarcomas with comparison to potentially related entities. *Mod Pathol* **30:** 797–809. doi:10.1038/modpathol.2017.11

Yoshihara K, Wang Q, Torres-Garcia W, Zheng S, Vegesna R, Kim H, Verhaak RG. 2015. The landscape and therapeutic relevance of cancer-associated transcript fusions. *Oncogene* **34:** 4845–4854. doi:10.1038/onc.2014.406

Zhang Y, Gong M, Yuan H, Park HG, Frierson HF, Li H. 2012. Chimeric transcript generated by *cis*-splicing of adjacent genes regulates prostate cancer cell proliferation. *Cancer Discov* **2:** 598–607. doi:10.1158/2159-8290.CD-12-0042

Zhang X, Hu J, Lu Jiade J, Gao J, Guan X, Kong L. 2017. Incidence patterns for myoepithelial carcinoma: a surveillance, epidemiology, and end results (SEER) study. *Transl Cancer Res* **6:** 441–449. doi:10.21037/tcr.2017.04.15